



# A climatological description of atmospheric CO<sub>2</sub> concentrations

François-Marie Bréon<sup>1</sup>, Frédéric Chevallier<sup>1</sup>, Michel Ramonet<sup>1</sup>

<sup>1</sup>Laboratoire des Sciences du Climat et de l'Environnement, CEA-CNRS-UVSQ, Université Paris-Saclay, Gif sur Yvette Cedex, 91191 France.

5 *Correspondence to:* François-Marie Bréon (breon@lsce.ipsl.fr)

**Abstract.** Atmospheric CO<sub>2</sub> concentrations show (i) a global trend, (ii) a seasonal cycle that varies with location and altitude and (iii) inter-annual and synoptic variability. The CO<sub>2</sub> atmospheric inversion of the Copernicus Atmosphere Monitoring Service (CAMS) constrained by surface measurements of the gas concentration provides a 4D (spatial+time) description of the CO<sub>2</sub> mixing ratio. A comparison of the CAMS modelling against AirCore profiles acquired over France indicates an accuracy on the order of 1 ppm (CO<sub>2</sub>) at most levels in the atmosphere with larger errors close to the surface. In this paper, we attempt a simple description of the concentration time series where the trend is provided by the Mauna Loa measurement dataset and the seasonal cycle is adjusted by an annual and semi-annual sinusoidal function. Most of the atmospheric concentration variability is captured by this simple modelling. Over France, the difference between simulated concentrations and in-situ (AirCore) measurements are on the order of 1.5 ppm over the free troposphere and higher. The evaluation against column concentration retrievals from the Total Carbon Column Observing Network (TCCON) indicates typical errors better than 1 ppm for the full atmospheric modelling and on the order of 1 ppm for the climatological fit.

The climatological product is updated in near-real time with the Mauna Loa measurements and may be therefore be used for a-priori information for ground-based and satellite based remote sensing of the column-averaged dry air mole fraction of CO<sub>2</sub> (XCO<sub>2</sub>).

## 20 1 Introduction

Carbon dioxide (CO<sub>2</sub>) is the dominant anthropogenic greenhouse gas and a key driver of ongoing climate change. Its atmospheric concentration has increased by approximately 50% since the beginning of the industrial era, with a current growth rate of about 2.5 ppm per year. Beyond this long-term increase, the spatial and temporal variability of CO<sub>2</sub> provides essential information for quantifying surface sources and sinks through atmospheric inversion methods (Ciais et al., 2010). This has motivated the development of extensive observational systems, including surface networks (Masarie and Tans, 1995; Franz et al., 2018), ground-based remote sensing (Wunch et al., 2011), and satellite missions (Crisp et al., 2004).

The variability of atmospheric CO<sub>2</sub> concentrations reflects the combined influence of surface fluxes and atmospheric transport. While interannual variations in natural and anthropogenic emissions exist, the observed time series are dominated by two



robust features: a globally coherent growth rate and a highly reproducible seasonal cycle. The latter arises primarily from  
30 biospheric exchange processes and exhibits strong spatial structure, with amplitudes and phase varying with latitude and  
altitude. In contrast, longitudinal variations are comparatively small due to efficient zonal mixing in the atmosphere.

These properties suggest that a large fraction of the observed variability of atmospheric CO<sub>2</sub> may be captured by a relatively  
simple representation combining a global trend and a spatially varying seasonal cycle (Keeling et al., 1976; Thoning et al.  
1989). Such an approach has been used for instance to gap-fill CO<sub>2</sub> observation time series (e.g., Masarie and Tans, 1995).  
35 Reuter et al. (2012) proposed an analytical model describing CO<sub>2</sub> concentrations as a function of time, latitude, and altitude  
using a set of 17 empirical parameters. However, the assumption of a constant growth rate limits its applicability in the context  
of the accelerated increase observed in recent years. In addition, its ability to reproduce the diversity of seasonal cycles across  
regions remains limited with the reduced set of parameters.

More recently, Laughner et al. (2023) developed an algorithm to generate prior CO<sub>2</sub> profiles for the GGG2020 retrieval  
40 framework used by the Total Carbon Column Observing Network (TCCON). Their approach combines observed growth rates  
from Mauna Loa and American Samoa with parameterizations of latitudinal gradients and seasonal variability. The algorithm  
estimates a mean difference between the concentrations at these sites and those at the location of interest based on the  
assumption that it is driven by emissions in the northern midlatitudes. The seasonal cycle is parameterized by a function that  
depends on the latitude and altitude. While this method improves the representation of large-scale gradients, evaluation against  
45 airborne and AirCore measurements reveals residual errors of up to several ppm, particularly in the Northern Hemisphere.

In this study, we revisit the problem of representing atmospheric CO<sub>2</sub> variability using a simple but physically grounded  
framework. Building on a high-resolution, multi-year reanalysis of atmospheric CO<sub>2</sub> from the Copernicus Atmosphere  
Monitoring Service (CAMS, <https://atmosphere.copernicus.eu/>), we show that most of the variability can be described by  
combining (i) a globally coherent growth rate derived from the Mauna Loa record and (ii) a seasonal cycle represented by two  
50 harmonics whose parameters vary in space.

This approach differs from previous analytical models in that it preserves spatial variability at the grid scale while maintaining  
a compact parameterization. It therefore provides a compromise between purely analytical formulations and full transport  
modelling. The resulting climatological description captures the dominant components of atmospheric variability while  
allowing the quantification of residual variability associated with synoptic transport and interannual fluctuations.

55 The objectives of this paper are threefold. First, we assess the ability of this simplified representation to reproduce the spatio-  
temporal variability of atmospheric CO<sub>2</sub> simulated by CAMS. Second, we evaluate both the full model and its climatological  
fit against independent observations from AirCore vertical profiles and column retrievals from the Total Carbon Column  
Observing Network (TCCON, Wunch et al., 2011). Third, we discuss the potential applications of this climatological product,  
in particular as prior information for remote sensing retrievals and as a reference framework for evaluating atmospheric CO<sub>2</sub>  
60 observations.



Section 2 describes the data and methods used in this analysis, both for model development and evaluation. Section 3 shows the results with a focus over France where a high density of AirCore profiles are available, but also an analysis at the global scale. Section 4 discusses the results and concludes

## 2 Data and methods

### 65 2.1 Atmospheric CO<sub>2</sub> modeling

We use a global reanalysis of the 3D atmospheric mole fractions and surface fluxes of CO<sub>2</sub> from the Copernicus Atmosphere Monitoring service (<https://atmosphere.copernicus.eu/>) based on an atmospheric inversion method. This reanalysis, version 22r1, was obtained by assimilating surface air-sample measurements from 159 sites over the globe in a global transport model. It covers the period between 1979 and 2022 at a global resolution of 2.50° in longitude and 1.27° in latitude, with 79 hybrid layers in the vertical, a relatively high resolution enabled by Graphics Processing Unit-accelerated model simulations (Chevallier et al., 2023). The atmospheric inversion system itself followed a variational formulation of Bayes's theorem, as described in Chevallier et al. (2010), with a single 44-year inversion window. It optimized the surface fluxes in each horizontal grid point of the transport model with a temporal resolution of 8 days, separately for daytime and night-time. Doing that, it also optimized the 4D atmospheric concentrations, which are the focus of this study.

### 75 2.2 Climatological fit

The analysis of CO<sub>2</sub> concentration time series shows a growth rate that is similar everywhere in the world at all atmospheric levels. This is the result of anthropogenic emissions, offset by about half by ocean and terrestrial carbon sinks (Friedlingstein et al., 2025), that lead to an increase of the concentrations, together with rapid atmospheric mixing. In addition, concentration time series show a seasonal cycle that results mostly from vegetation uptake and respiration and also from oceanic and anthropogenic fluxes. The amplitude and shape of this seasonal cycle varies spatially (e.g., Masarie and Tans, 1995). We therefore suggest to build a climatological fit of the modeled time series as a general trend that is described by the iconic Mauna Loa time series maintained by the Scripps Institution of Oceanography and NOAA (<https://gml.noaa.gov/ccgg/trends/data.html>) and a seasonal cycle that is described by two harmonics:

$$[CO_2]_{l,p}(t) = [CO_2]^{ML}(t) + A_{l,p}^0 + A_{l,p}^1 \cos(\omega(t + d_{l,p}^1)) + A_{l,p}^2 \cos(2\omega(t + d_{l,p}^2)) \quad (1)$$

85 where  $[CO_2]_{l,p}(t)$  is the CO<sub>2</sub> dry air mole fraction at location  $l$ , pressure  $p$  and time  $t$ ;  $[CO_2]^{ML}$  is the de-seasonalized time series of CO<sub>2</sub> dry air mole fraction at the Mauna-Loa observatory,  $\omega (=2\pi/365)$  is used to generate an annual cycle, and  $A^0$ ,  $A^1$ ,  $A^2$   $d^1$  and  $d^2$  are free parameters for a best fit of the data.

Note that the formulation of Equation (1) is equivalent to



$$[CO_2]_{l,p}(t) = [CO_2]^{ML}(t) + A_{l,p}^0 + A_{l,p}^1 \cos(\omega t) + A_{l,p}^2 \sin(\omega t) + A_{l,p}^3 \cos(2\omega t) + A_{l,p}^4 \sin(2\omega t) \quad (2)$$

90 which is easier to optimize against observations, as it is a linear combination of the 5 free parameters  $A^0$  to  $A^4$ .

We use a similar approach for the column-averaged dry air mole fraction of CO<sub>2</sub> (XCO<sub>2</sub>) as :

$$[XCO_2]_l(t) = [CO_2]^{ML}(t) + B_l^0 + B_l^1 \cos(\omega t) + B_l^2 \sin(\omega t) + B_l^3 \cos(2\omega t) + B_l^4 \sin(2\omega t) \quad (3)$$

In the following, we analyze the ability of this simple parameterization to reproduce the concentration time series and quantify the error of both the full atmospheric modeling and its climatological fit against independent observations.

95 Note that, once the fit parameters have been adjusted, the CO<sub>2</sub> concentration can be extrapolated in time using updated Mauna Loa time series. This assumes that the seasonal cycle does not change dramatically, which is expected. The concentration can also be extrapolated in time for a few years, on the basis of a typical atmospheric growth rate of CO<sub>2</sub> ( $\approx 2.5$  ppm/year in recent years).

### 2.3 AirCore measurements

100 For the evaluation of both simulations, we use a set of 80 AirCore profiles that have been acquired over France between 2016 and 2023. AirCore is a technique developed in 2010 at NOAA/ESRL which makes it possible to sample the atmosphere from the surface to  $\approx 30$  km (Karion et al., 2010). The concept proposed by NOAA was copied in France (Membrive et al., 2017), and LSCE has a program of monthly sampling of the atmosphere. The balloons are launched from a location close to the Trainou instrumented site located northeast of the city of Orléans. This site is part of the TCCON and Integrated Carbon  
105 Observation System (ICOS) networks. The air sampling is made on the descending portion of the flight. Figure 1 shows the locations of the sampling apparatus return to the ground which are all located within the French territory.

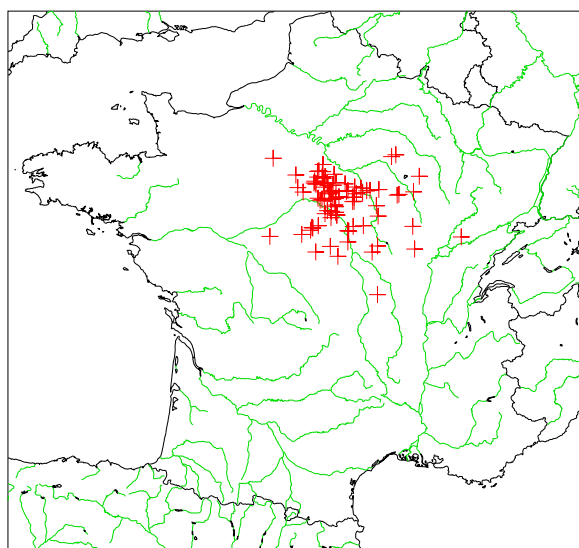




**Figure 1: Location of the landings for the AirCore samplings that are used in this paper for evaluation.**

110 For each AirCore profiles, we sampled the model at the location and time of the ground return. The AirCore measurements were averaged vertically at the scale of the model layers. The averages were then used to compute the concentration difference between the observation and the model.

## 2.4 TCCON

TCCON is a global network of ground-based Fourier Transform Infrared (FTIR) spectrometers that provide precise and  
115 accurate measurements of the total column abundances of atmospheric greenhouse gases, including CO<sub>2</sub> (Wunch et al., 2011). TCCON observations are based on high-resolution solar absorption spectra recorded in the near-infrared and are analyzed using a common retrieval framework.

The network delivers XCO<sub>2</sub> with a precision better than 1 ppm and a trueness about 0.4–0.8 ppm, supported by regular calibration and validation activities. TCCON data are widely used as a reference for the evaluation and calibration of satellite  
120 CO<sub>2</sub> retrievals, as well as for studies of carbon cycle variability and atmospheric transport.

TCCON provides XCO<sub>2</sub> column-averaged that serve as a primary validation standard for space-based greenhouse-gas missions. Owing to its long-term stability, standardized retrieval algorithms, and traceability to the WMO scale (through comparisons with aircraft and AirCore measurements), TCCON plays a central role in assessing biases, temporal stability, and regional representativeness of satellite CO<sub>2</sub> products.

125 In this paper, we use TCCON estimates that have been processed in November 2023 (GGG2020 version). Further information about TCCON, its measurements and processing can be found on the wiki page <https://tcon-wiki.caltech.edu/>. The TCCON XCO<sub>2</sub> estimates are used here to evaluate both the CAMS modelling described in 2.1 and its climatological fit described in 2.2.

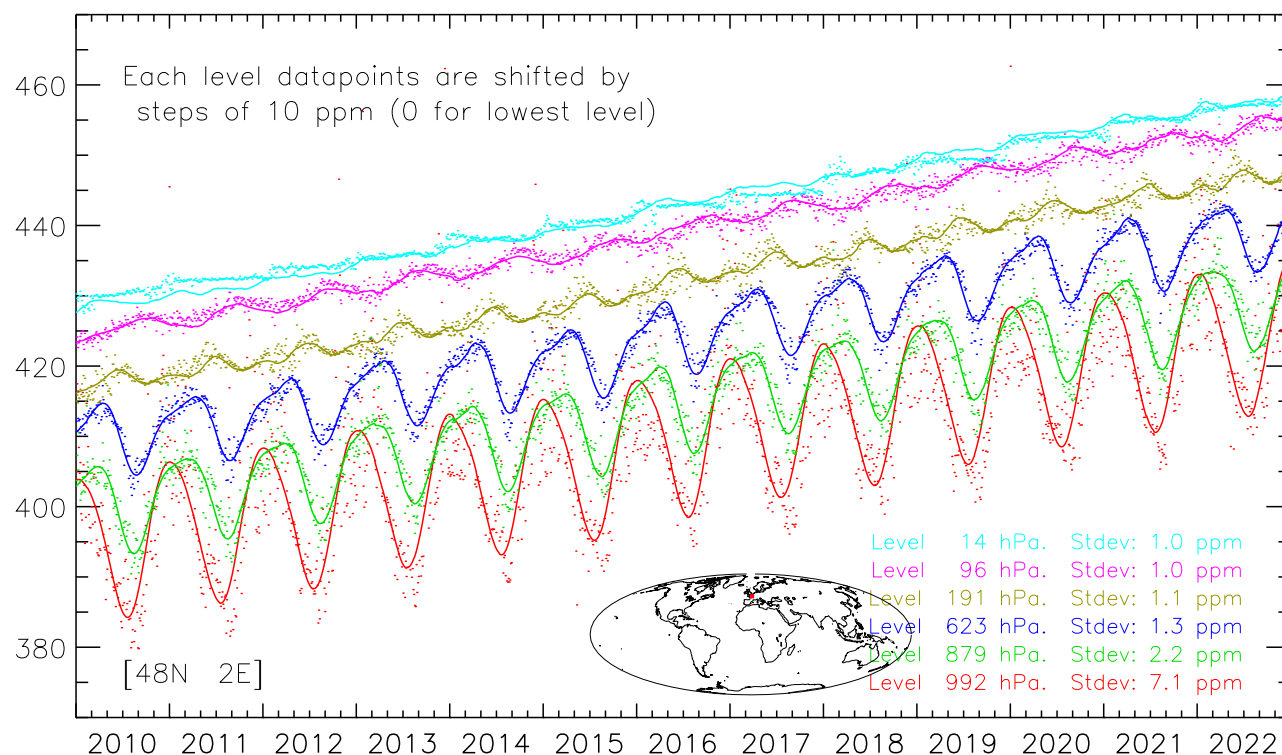
## 3 Results

### 130 3.1 Time series

Figure 2 shows the time series of CAMS modelled atmospheric concentrations and climatological fit using Equation (2). The figure illustrates the growth rate that is identical at each level of the atmosphere, and the annual cycle that is much more pronounced in the low atmospheric layers than in the atmosphere. The seasonal cycle takes different shapes depending of the atmospheric layers, and it appears that two harmonics are sufficient to describe these shapes. Figure 2 is for one location, that  
135 is chosen here because it is at the centre of the AirCore samples described in 2.3 (see Figure 1), but similar conclusions can be drawn from the results at other locations, although the seasonal cycle amplitude is much less in the southern hemisphere (see Figure 5).



As expected, there is some scatter around the climatological fit. This scatter is linked to inter-annual as well as synoptic variabilities. For this particular location, it is on the order of 1 ppm in the mid and high atmosphere (above 700 hPa) but higher in the low atmospheric layers, in direct interaction with CO<sub>2</sub> fluxes at the surface. The misfit is a quantification of the variability of atmospheric CO<sub>2</sub> concentrations that cannot be described by the climatology. In the following, we evaluate both the CAMS modelling and its climatologic fit against independent measurements. Note that neither the AirCore profiles nor the TCCON measurements have been used to constrain the CAMS modelling. They are therefore truly independent from the modeled data.



145 **Figure 2: Time series of the CAMS modelled concentrations at various atmospheric levels in the atmosphere (dots) and best fit adjustment (lines) using analytical equation (1). The RMS errors for the fit are provided at the lower-right of the figure. This is for the location [48N 2E] which is at the center of the AirCore samples described in section 2.3. Each level datapoints and fit have been shifted by 10 ppm to avoid overlap (no shift for the lowest level).**

### 3.2 Evaluation against AirCore profiles

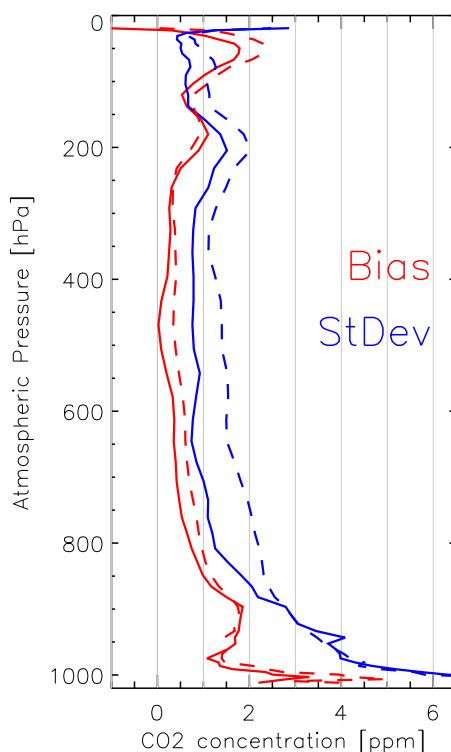
150 We use the 80 AirCore profiles described in Section 2.3 to evaluate both the CAMS modelling and its climatological fit. The model vertical sampling uses sigma coordinates that vary with the surface pressures. All model-AirCore comparisons are done at the sigma levels and we account for the surface pressure variations to sample the AirCore profiles at the corresponding model layers. The results are shown for a standard surface pressure of 1013 hPa.



The biases are very similar for the model and its climatological fit, as expected. It is less than 0.5 ppm for the mid atmosphere but is significantly larger (1-2 ppm) both in the high atmosphere (above 200 hPa) and in the low atmosphere (below 850 hPa). The standard deviation (STDDEV) of the model is less than 1 ppm in the middle atmosphere (between 300 and 800 hPa) but takes large values ( $\approx 2$  ppm) in the mixing layer. The standard deviation of the climatological fit is close to 1.5 ppm within the free troposphere, and takes large values in the low atmosphere, consistently to that of the CAMS product.

The larger STDDEV values of the climatological fit than the model are expected as the former cannot reproduce neither the inter-annual anomalies nor the synoptic variability. Nevertheless, the 2 ppm standard deviation is much less than both the growth over the analysis period and the amplitude of the seasonal cycle, which confirms that the climatological fit reproduces most of the CO<sub>2</sub> concentration variability. In addition, the standard error of the climatological fit is larger, but on the same order of magnitude as the typical difference between the CAMS modelling and its climatological fit.

We acknowledge however that the statistics reported here may not be representative of the full globe. On the one hand, the synoptic variability, which the climatological fit cannot reproduce, is larger at mid latitudes than it is in the tropical regions. On the other hand, there is a high density of CO<sub>2</sub> monitoring stations in Western Europe and their measurements provide a constrain for the CAMS modelling that is not available everywhere. As a consequence, further evaluation over a more distributed set of measurements is necessary.



170 **Figure 3: Statistical comparison (Red: Biases; Blue: Standard deviation) of the AirCore vertical samples against both the CAMS modelling (plain lines) and its climatological fit (dashed lines).**



### 3.3 Evaluation against TCCON

175 TCCON stations are distributed over the globe which provides some indication on the spatial variability of the model performance. However, the TCCON standard products only provide a total column estimate with no indication on the vertical distribution. We therefore evaluate the total CO<sub>2</sub> column concentration from the CAMS modeling as well as its climatological fit as in Equation (3). The column is computed with a constant vertical weighting without accounting for the vertical sensitivity of the remote sensing product.

180 The results shown in Figure 4 confirm the spatial variability of the statistics with smaller errors in the southern hemisphere and in the tropics than in the mid and high latitudes of the Northern hemisphere. The errors are on the order of 1 ppm. As expected, the errors are larger for the climatological fit than they are for the CAMS modeling, with three exceptions (Hefei, Manaus and Darwin) where they are almost identical.

185 Note that the prior used for the TCCON estimate (Laughner et al. (2023) shows a difference with respect to the posterior value that is significantly larger than that obtained with the climatological fit. This strongly indicates that this fit could offer a better prior for this inversion. However, the TCCON posterior value is loosely constrained by its prior, so that the use of a better prior may not change significantly the TCCON XCO<sub>2</sub> estimates.

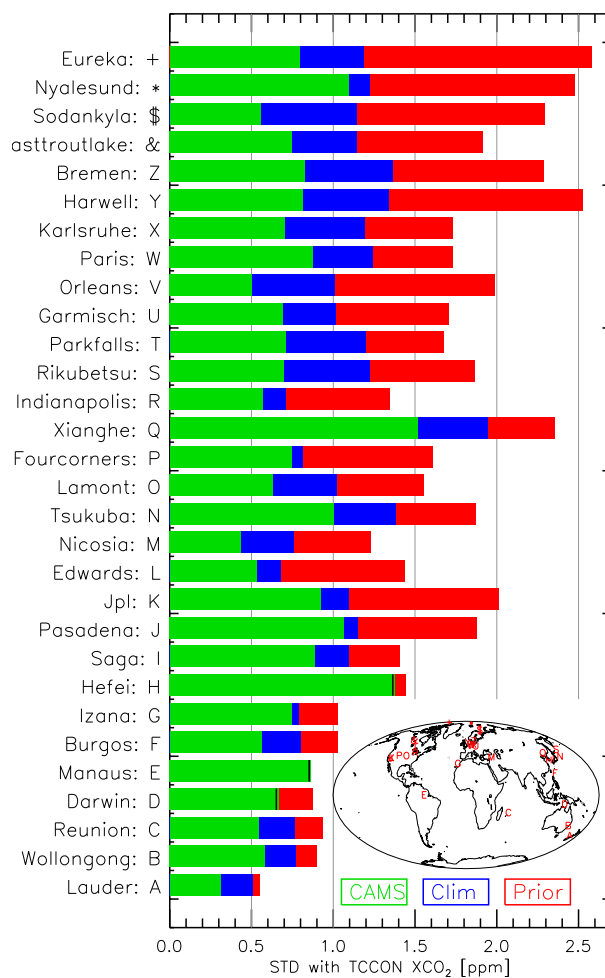


**Figure 4: Statistical comparison (Standard deviation) of the TCCON total column estimates the CAMS modelling (green, the climatological fit (blue) and the GGG2020 prior used for the TCCON retrieval (red). The stations are sorted according to their latitude.**

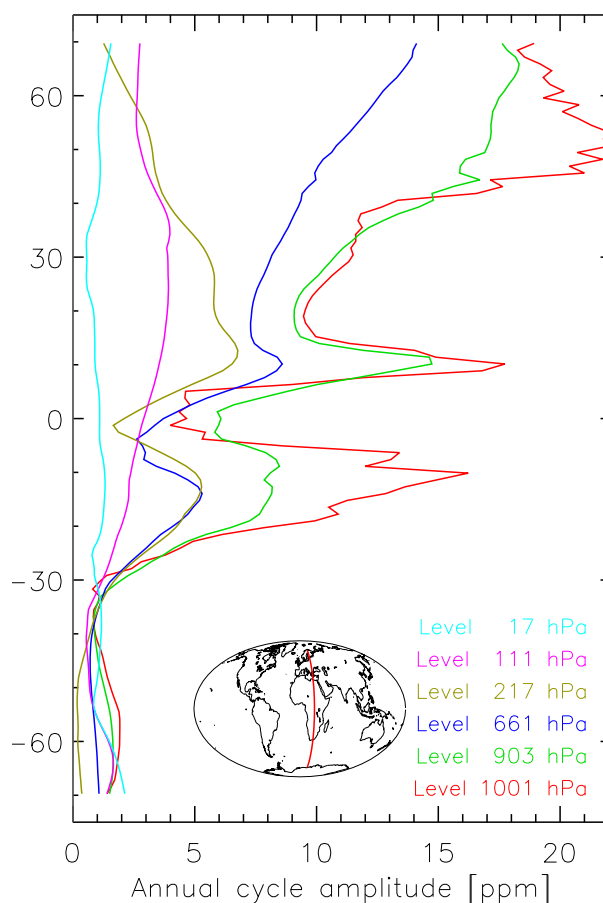
190 **3.4 Amplitude of the seasonal cycle**

Figure 5 shows the amplitude of the CO<sub>2</sub> seasonal cycle at various levels in the atmosphere along longitude 25°E, chosen to maximize the coverage of land surfaces. The amplitude of the cycle is computed directly from the four  $A^i$  coefficients ( $A^1$  to  $A^4$ ) of Equation (2). As expected, the seasonal cycle amplitude is larger in the low atmospheric layers than it is higher up. The seasonal cycle varies also strongly with the latitude : It is less than 2 ppm south of 30°S but takes values of more than 10 ppm north of 10°N, a difference which is a direct consequence of the fraction of land surfaces at the mid and high latitudes of the two hemispheres. Note that the seasonal cycle is rather high over the Sahara Desert (15-30° N) despite the absence of vegetation. It results from the transport of CO<sub>2</sub> from other regions of the northern hemisphere with vegetation covers that

195

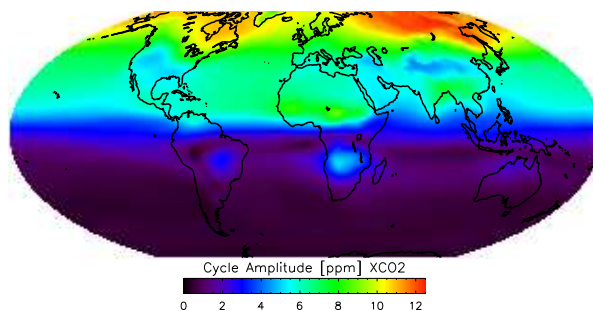


drives a large seasonal cycle of the CO<sub>2</sub> fluxes. In the high atmosphere, the seasonal cycle amplitude is smaller than in the low atmospheric levels but remains significant, up to 5 ppm. The seasonal cycle in the high atmosphere is not necessarily in phase with that observed at lower atmospheric levels, as for instance shown in Figure 2.



**Figure 5: Amplitude of the CO<sub>2</sub> seasonal cycle at various atmospheric levels as a function of latitude along the 25°E meridian.**

Figure 6 shows the amplitude of the XCO<sub>2</sub> seasonal cycle. The range of variation is large with values less than 2 ppm in most of the Southern hemisphere (with some exception over South-America, Africa and Northern Australia) and up to 12 ppm over Siberia. The structure is mostly zonal, with a strong South-North gradient, although larger values are observed over the Eastern part of the continents (with respect to the Western part) at the northern mid and high latitudes. Regions of high elevation also show a reduced seasonal cycle of CO<sub>2</sub> with respect to other regions of the same latitude.



210

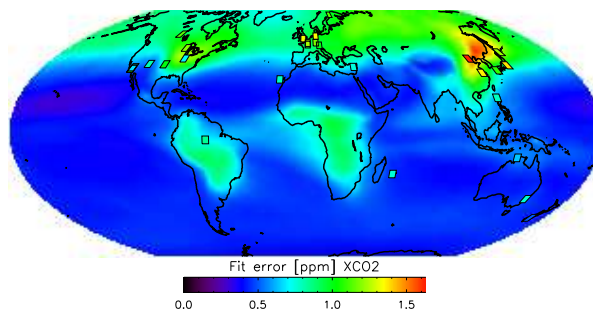
**Figure 6: Amplitude of the XCO<sub>2</sub> seasonal cycle.**

### 3.5 Error of the Fit

Figure 2 shows time series of CAMS simulations together with the climatological fit at various levels in the atmosphere. A similar analysis (not shown) can be performed over the XCO<sub>2</sub> time series as in Equation (3). Figure 7 shows the RMS error of the fit as a function of location. Typical values are between 0.5 and 1.6 ppm with the smallest values observed in the Pacific, close to Hawaiï and the Mauna Loa observatory, and the largest value over the North East of China. Over the northern hemisphere, the error of the fit is much smaller than the seasonal cycle amplitude (Figure 6) indicating that the seasonal cycle is fairly constant from year to year, which is a main hypothesis of the climatological fit developed in this paper. The error of fit is less than 1 ppm over most of the oceans but takes larger values over the continents of the Northern hemisphere where vegetation fluxes, together with synoptical variability in the atmospheric transport, leads to day-to-day variations (Figure 2) that cannot be reproduced by the climatology.

220

Overlaid on Figure 7 are the standard deviations of the differences between the climatological analysis and the TCCON retrievals. In general, the typical differences with TCCON are slightly larger (a few tenths of a ppm) than the differences with CAMS but the spatial structure is consistent with the largest and smaller values found in the same areas.



225

**Figure 7: RMS error [ppm] between the XCO<sub>2</sub> CAMS simulation and the climatological fit. The symbols overlaid on the map are at the location of the TCCON stations and indicate the error of the climatological fit with respect to the TCCON measurement, as in Figure 4.**

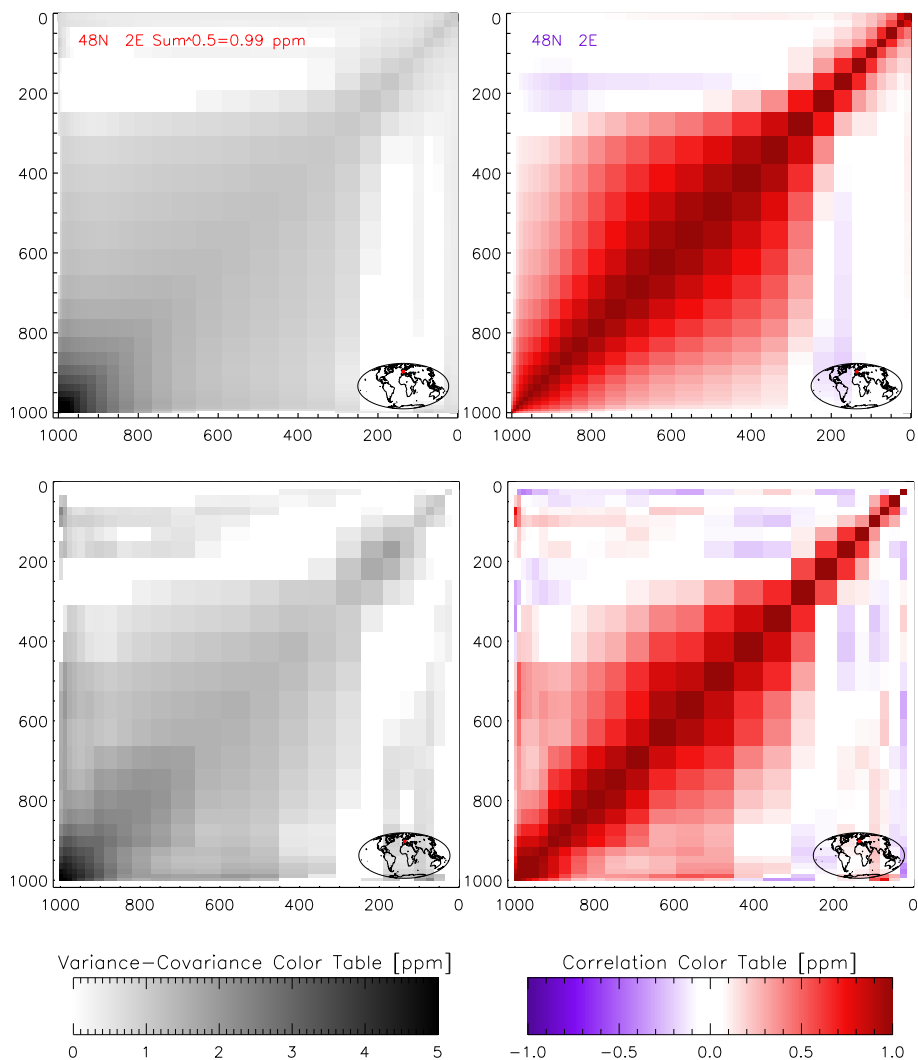


### 3.5 Vertical Covariance

230 We now analyze the vertical covariance of the climatological fit errors. One approach is to use the AirCore profiles described  
in Section 2.3 and analyzed in 3.2. There are 80 profiles available, which is sufficient for a statistical analysis. We also  
attempted an analysis for each of the 4 meteorological seasons, but the sample is then insufficient to draw firm conclusions.  
The differences between the AirCore profiles and the climatological fit are computed at the model level resolution and used to  
compute variance-covariances and vertical correlations, which are shown in Figure 8. This can be done only at the location of  
235 the AirCore profiles (Figure 1).

The other approach is to use the CAMS simulation as the truth, compute the error at each time step and atmospheric level, and  
then compute a vertical variance-covariance from the time series of the differences. This shall be done independently for each  
of the model grid cell. In Figure 8, we show the result for the model grid cell [48N; 2E] at the center of the AirCore samples  
(Figure 1), but similar analysis can be produced over all grid cells.

240 As expected, there is some vertical correlation on the errors (both in the model and in the AirCore samples) which leads to  
positive correlation and covariances. Some weak negative correlations are observed between the stratosphere and the  
troposphere. The two methods lead to rather similar results. The variances-covariances have the same order of magnitude,  
with larger values in the low atmosphere. There is a local maximum on the covariance around  $\approx 150$  hPa which corresponds to  
the troposphere-stratosphere transition, whose height may vary with a temporality that is poorly reproduced by the modeling.  
245 The vertical correlations estimates are rather similar, although slightly larger when computed against the model than against  
the AirCores. Overall, for this particular location, it appears that the error variance-covariance of the climatological fit,  
evaluated against the in-situ measurements, can be approximated by the value derived from the CAMS analysis.



250

**Figure 8: Variance Covariance (left) and correlation matrices of the CO<sub>2</sub> concentration error. The first line is based on the difference between the CAMS simulations and the climatological fit. The second line is based on the difference between the AirCore profiles and the climatological fit. The figures on the left show the square root of the covariance (bound at zero), expressed in ppm.**

## 4 Discussion

### 255 4.1 Physical interpretation

The results demonstrate that a large fraction of the atmospheric CO<sub>2</sub> variability can be represented by the combination of (i) the growth rate measured at the iconic Mana Loa station and (ii) a stationary seasonal cycle described by two harmonics. This



confirms that, at first order, the temporal evolution of atmospheric CO<sub>2</sub> is dominated by large-scale processes that are spatially coherent: the anthropogenic trend and the biospheric seasonal exchange.

260 The success of the approach reflects two key properties of atmospheric CO<sub>2</sub>:

- Rapid large-scale mixing, which ensures that the long-term growth rate is nearly uniform across latitudes and vertical levels.
- Strong periodicity of biospheric fluxes, particularly in the Northern Hemisphere, which produces a remarkably regular seasonal cycle whose shape is well captured by annual and semi-annual harmonics.

265 The fact that the residual variability is typically below 1–2 ppm in the free troposphere indicates that interannual changes in fluxes and synoptic transport, while detectable, remain second-order compared to the seasonal amplitude of the concentration (up to 10–12 ppm at northern mid-latitudes).

However, the degradation of performance in the planetary boundary layer highlights the intrinsic limitation of any climatological approach: surface flux variability and boundary-layer dynamics introduce short-term fluctuations that cannot

270 be captured by stationary harmonics.

#### 4.2 Relation to previous empirical background models

The approach developed here has similarities with empirical background models such as that proposed by Reuter et al. (2012) and Laughner et al. (2023), which described atmospheric CO<sub>2</sub> using a simple analytical formulation and a reference to the

275 Mauna Loa and American Samoa observations for the latter. Our approach is slightly more complex however. Indeed, Reuter et al. used only 17 coefficients to describe the CO<sub>2</sub> variability over the full Earth and atmospheric levels, while the approach of Laughner et al. (2023) is purely analytical with a set of empirical values embedded within the equations. Our approach uses only 5 coefficients, but these are different for each grid point and atmospheric levels. Thus, while the two former approaches are purely analytical and can be implemented as a simple analytical function, our approach requires a 25 Mo dataset as input.

We have compared the performance of these approaches. Although the fully analytical functions do reproduce the main variations of atmospheric CO<sub>2</sub>, its performance appears limited compared to our approach. Reuter et al. (2012) assumed a constant growth rate in the atmosphere while the true growth has accelerated in the past decade. This is corrected in the method of Laughner et al. (2023) that uses observations to constrain the mean trend, but the evaluation against TCCON shows that our approach leads to significantly lower errors. Besides, Laughner et al. assumed no variation of the concentrations along the longitudes, which is a strong limitation, in particular for the low atmospheric levels.

285 The analytical approach of Reuter (2012) or Laughner et al. (2023) may be sufficient when only a rough estimate of the CO<sub>2</sub> profile is needed. Our approach brings additional accuracy at the cost of some complexity.



### 4.3 Implications for satellite retrievals

Our simple modelling of the atmospheric CO<sub>2</sub> could be used as an accurate prior for satellite retrievals of the atmospheric concentration. Indeed, the validation against both AirCore and TCCON station has shown an accuracy better than 1.5 ppm on  
290 XCO<sub>2</sub>, and a reasonable description of the vertical profile. This suggests that the proposed formulation could serve as a physically informed prior for column or profile retrievals. Because the formulation is linear in its parameters, it can be easily implemented and can also be updated as new Mauna Loa data become available. Besides, as the de-seasonalized growth rate does not vary strongly from month to month, the Mauna Loa time series can be extrapolated in time over a few months with no significant added error on the climatological product.

295 Importantly, the vertical covariance analysis indicates that errors of the climatological fit are vertically correlated, especially within the troposphere. This has consequences for the specification of background error covariance matrices in inversion systems. The similarity between covariance structures derived from CAMS and from AirCore comparisons suggests that the model-based estimate provides a reasonable approximation of real atmospheric variability. Thus, the covariance matrices, which have been derived based on the CAMS vs analytical fit differences, may be used for the satellite-based inversions of the  
300 CO<sub>2</sub> profiles.

### 4.4 Potential for satellite retrieval validation

The proposed climatological product may also provide a useful framework for a first evaluation of space-borne CO<sub>2</sub> retrievals. Because it captures the dominant components of atmospheric variability — namely the long-term trend and the stationary seasonal cycle — it defines a physically consistent baseline against which satellite products can be evaluated. Obviously, the  
305 satellite products aim at improving our knowledge in the atmospheric concentration, and are therefore designed to achieve an accuracy that is higher than that of the climatological product. Yet, a comparison of the retrievals against this climatology may be used as a first validity check during the commissioning phase.

In regions where the residual variability relative to the climatology is small (e.g. remote oceanic areas, tropical regions, or the Southern Hemisphere), the atmospheric state is largely controlled by well-mixed background conditions. In such regions,  
310 discrepancies between satellite retrievals and the climatological estimate are more likely to reflect retrieval biases, instrumental effects, or forward-model errors rather than unresolved atmospheric variability. These areas therefore offer favorable conditions for assessing systematic errors and long-term stability.

Conversely, in regions where the residual variability is large — in particular over continental mid- and high latitudes of the Northern Hemisphere — synoptic transport, boundary-layer dynamics, and heterogeneous surface fluxes introduce short-term  
315 fluctuations that are not captured by the climatological representation. In these areas, differences between satellite products and the climatological estimate cannot be interpreted solely as retrieval errors, since part of the discrepancy may arise from real atmospheric variability. The spatial structure of the fit residuals thus provides an objective indicator of where satellite validation can rely on a stable background and where additional caution is required.



320 More generally, the product may help separate two components of satellite error diagnostics: (i) systematic biases relative to a well-characterized background, and (ii) representation errors linked to unresolved atmospheric variability. This distinction is particularly relevant for the evaluation of high-precision missions targeting sub-ppm accuracy.

#### 4.5 Limitations of the approach, and potential for improvements

Several limitations of the approach must be acknowledged, and offer potential for improvements.

325 Our approach uses the measurements at Mauna Loa to describe the mean growth rate at all point over the globe. The near-uniform growth rate observed across latitudes and vertical levels is consistent with characteristic tropospheric mixing times of a few weeks zonally, a few months meridionally within a hemisphere, and approximately one year between hemispheres (Jacob et al. 1997). The one-year time scale for inter-hemispheric exchange suggests the use of a different growth rate for the North and South hemispheres. Thus, over the southern hemisphere, one could replace the Mauna Loa time series by that from American Samoa, operated by NOAA-CMDL (Thoning et al., 2025) or the observations from Amsterdam Island operated by  
330 LSCE.

The method assumes that the seasonal cycle does not change significantly over the analysis period. Yet, observations of surface concentrations of CO<sub>2</sub> over several decades indicate an increase of the amplitude of the seasonal cycle in the Northern hemisphere (Graven et al., 2013; Piao et al., 2017). Our approximation appears valid over 13 years, but long-term changes in biospheric phenology exacerbated by climate change, could eventually invalidate this assumption. A new fit against updated  
335 time series may therefore become necessary in the future to account for these changes.

Our approach shows large errors in the lower atmospheric layers where surface fluxes and mixing heights vary rapidly. A purely harmonic representation cannot reproduce synoptic variability, frontal passages, or localized flux events. This is inherent to the climatological approach.

We have validated the CAMS and climatological fit against AirCore over a single region which may not be representative of  
340 the whole globe. This region (central France) shows a large seasonal cycle and synoptic variability, when compared to other regions of the globe, as shown in Figure 6 and 7. Yet, other regions (such as Siberia and Eastern Asia) show even larger cycle amplitude and variabilities which may be difficult to handle by our simple approach. In addition, the CAMS modelling over western Europe is well constrained by a high density of surface observations that is not available elsewhere. One may therefore question the representativeness of some results. Further evaluation could use other AirCore regular samples, such as those  
345 from NOAA (Baier et al., 2023) or the one in Sodankyla, Finland.

For the comparison against TCCON, we did not account for averaging kernels. While acceptable for a first-order assessment, this simplification may slightly bias the interpretation of TCCON comparisons. A more precise evaluation of the precision of CAMS and its climatological fit should account for the variations linked to the averaging kernels.



## 5 Conclusion

350 In this paper, we have developed and evaluated a climatological representation of atmospheric CO<sub>2</sub> variability at seasonal and interannual scales based on a multi-year 4D reanalysis. This representation is available in near-real time thanks to the near-real-time availability of the CO<sub>2</sub> measurements at the Mauna Loa station, operated by the Scripps Institution of Oceanography and NOAA. The analysis confirms that, at first order, atmospheric CO<sub>2</sub> variability is dominated by a globally coherent growth rate and a largely stationary seasonal cycle driven by biospheric fluxes. The seasonal component can be robustly represented

355 using only two harmonics, showing that most of the observed variability can be described with a limited number of parameters. Evaluation against independent AirCore vertical profiles and TCCON column retrievals demonstrates that the typical representation error of the climatological fit is on the order of 1–1.5 ppm for XCO<sub>2</sub>, with smaller errors over the Southern Hemisphere and oceanic regions, and larger residuals over northern continental areas. These results confirm that a substantial fraction of atmospheric CO<sub>2</sub> variability is highly regular in space and time.

360 The residual deviations from the climatology, typically around 1 ppm and regionally up to 1.5 ppm, define the scale of atmospheric variability that cannot be captured by a stationary representation. This provides a physically based benchmark for assessing the accuracy requirements of satellite retrievals and highlights the level of systematic precision needed for applications in atmospheric inversions.

Beyond its analytical interest, the climatological product offers a compact and practical framework for representing

365 atmospheric CO<sub>2</sub> fields and their associated error structures. By separating the dominant climatological signal from higher-frequency variability, it may facilitate the evaluation of satellite observations, the specification of prior information in retrieval algorithms, and the interpretation of regional CO<sub>2</sub> anomalies. The climatological product may also be used for other purposes when an estimate of the CO<sub>2</sub> concentration is needed, in particular in near-real-time. For instance, it is used among other predictors by the Copernicus Marine Environment Service (<https://marine.copernicus.eu/>) to estimate the surface ocean

370 fugacity and air-sea fluxes about one month behind real time (Chau et al. 2024).

The use of the climatological product relies on a dataset (netCDF file) that provides the 5 parameters on a latitude-longitude grid and for 79 atmospheric levels. The file is 25 Mbytes. In addition, the analysis led to variance-covariance matrices for each of the model grid points. The corresponding file will be used as prior information for the derivation of CO<sub>2</sub> profiles based on the MicroCarb satellite measurements. The file is 400 Mbytes and can be distributed for other uses.

## 375 Data availability

Two NetCDF files have been created in the context of this study and are available for any use. The first one contains the 5  $A^i$  coefficients in Equation (2) on a lat-lon-pressure grid. The second one contains the vertical variance-covariance matrices (Figure 8) on a lat-lon grid. They are available from

<https://sharebox.lsce.ipsl.fr/index.php/s/xGCD36KuYmN3OcZ>



380 <https://sharebox.lsce.ipsl.fr/index.php/s/dT5etwySTrWgIBN>

### Author contributions

FMB created the priors code, carried out the validation, and led the writing of the manuscript. FC developed the CAMS modelling that is used in the paper. MR developed the AirCore program that is used for the product evaluation. FMB prepared the manuscript with contributions from all co-authors.

### 385 Competing interests

The authors declare no competing interest

### Acknowledgements

The authors are grateful to the teams and funding bodies that make possible the measurements from the TCCON network.

### References

- 390 Baier, B.C., Sweeney, C., Chen, H. Chapter 8 - The AirCore atmospheric sampling system. In: Nalli, N.R. (Ed.), *Field Measurements for Passive Environmental Remote Sensing*. Elsevier, pp. 139–156, 2023.
- Chau, T.-T.-T., Chevallier, F., & Gehlen, M.: Global analysis of surface ocean CO<sub>2</sub> fugacity and air-sea fluxes with low latency. *Geophysical Research Letters*, 51, e2023GL106670. <https://doi.org/10.1029/2023GL106670>, 2024.
- Chevallier, F., P. Ciais, T. J. Conway, T. Aalto, B. E. Anderson, P. Bousquet, E. G. Brunke, L. Ciattaglia, Y. Esaki, M. Fröhlich, 395 A.J. Gomez, A.J. Gomez-Pelaez, L. Haszpra, P. Krummel, R. Langenfelds, M. Leuenberger, T. Machida, F. Maignan, H. Matsueda, J. A. Morguí, H. Mukai, T. Nakazawa, P. Peylin, M. Ramonet, L. Rivier, Y. Sawa, M. Schmidt, P. Steele, S. A. Vay, A. T. Vermeulen, S. Wofsy, D. Worthy: CO<sub>2</sub> surface fluxes at grid point scale estimated from a global 21-year reanalysis of atmospheric measurements. *J. Geophys. Res.*, 115, D21307, doi:10.1029/2010JD013887, 2010.
- 400 Chevallier, F., Lloret, Z., Cozic, A., Takache, S., & Remaud, M.: Toward high-resolution global atmospheric inverse modelling using graphics accelerators. *Geophysical Research Letters*, 50, e2022GL102135, 2023.
- Ciais, P., Rayner, P., Chevallier, F. *et al.* Atmospheric inversions for estimating CO<sub>2</sub> fluxes: methods and perspectives. *Climatic Change* **103**, 69–92: <https://doi.org/10.1007/s10584-010-9909-3>, 2010.



- 405 Crisp, D. et al., The Orbiting Carbon Observatory (OCO) mission, *Advances in Space Research*, (34) 4, <https://doi.org/10.1016/j.asr.2003.08.062>, 2004.
- Franz, D.; Acosta, M.; Altimir, N.; Arriga, N.; Arrouays, D.; Aubinet, M., et al. : Towards long-term standardised carbon and greenhouse gas observations for monitoring Europe's terrestrial ecosystems: a review. *International Agrophysics*, 32(4), 439-455. OSTI ID: 1494095. <http://dx.doi.org/10.1515/intag-2017-0039>, 2018.
- 410 Friedlingstein, P., Le Quéré, C., O'Sullivan, M. et al. Emerging climate impact on carbon sinks in a consolidated carbon budget. *Nature* **649**, 98–103: <https://doi.org/10.1038/s41586-025-09802-5>, 2026.
- Graven, H. D., Keeling, R. F., Piper, S. C., Patra, P. K., Stephens, B. B., Wofsy, S. C., ... Bent, J. D.: Enhanced seasonal exchange of CO<sub>2</sub> by northern ecosystems since 1960. *Science*, 341, 1085–1089, 2013.
- 415 Jacob, D. J., Prather, M. J., Rasch, P. J., Shia, R.-L., Balkanski, Y. J., Beagley, S. R., Bergmann, D. J., Blackshear, W. T., Brown, M., Chiba, M., Chipperfield, M. P., de Grandpré, J., Dignon, J., Feichter, J., Genthon, C., Grose, W. L., Kasibhatla, P. S., Köhler, I., Kritz, M. A., Law, K. S., Penner, J. E., Ramonet, M., Reeves, C. E., Rotman, D. A., Stockwell, D. Z., Van Velthoven, P. F. J., Verver, G. H., Wild, O., Yang, H., & Zimmermann, P.: Evaluation and intercomparison of global atmospheric transport models using <sup>222</sup>Rn and other short-lived tracers. *Journal of Geophysical Research: Atmospheres*, 102(D5), 5953–5970. <https://doi.org/10.1029/96JD02955>, 1997.
- Karion, A., C. Sweeney, P. Tans, T. Newberger : AirCore: an innovative atmospheric sampling system, *J. Atmos. Ocean. Technol.*, 27, 1839-1853, doi : 10.1175/2010JTECHA1448.1, 2010.
- 420 Keeling, C.D., Bacastow, R.B., Bainbridge, A.E., Ekdahl, C.A., Jr., Guenther, P.R., Waterman, L.S. and Chin, J.F.S.: Atmospheric carbon dioxide variations at Mauna Loa Observatory, Hawaii. *Tellus*, 28: 538-551. <https://doi.org/10.1111/j.2153-3490.1976.tb00701.x>, 1976.
- 425 Laughner, J. L., Roche, S., Kiel, M., Toon, G. C., Wunch, D., Baier, B. C., Biraud, S., Chen, H., Kivi, R., Laemmle, T., McKain, K., Quéhé, P.-Y., Rousogonous, C., Stephens, B. B., Walker, K., and Wennberg, P. O.: A new algorithm to generate a priori trace gas profiles for the GGG2020 retrieval algorithm, *Atmos. Meas. Tech.*, 16, 1121–1146, <https://doi.org/10.5194/amt-16-1121-2023>, 2023.
- 430 Laughner, J. L., Toon, G. C., Mendonca, J., Petri, C., Roche, S., Wunch, D., Blavier, J.-F., Griffith, D. W. T., Heikkinen, P., Keeling, R. F., Kiel, M., Kivi, R., Roehl, C. M., Stephens, B. B., Baier, B. C., Chen, H., Choi, Y., Deutscher, N. M., DiGangi, J. P., Gross, J., Herkommer, B., Jeseck, P., Laemmle, T., Lan, X., McGee, E., McKain, K., Miller, J., Morino, I., Notholt, J., Ohyama, H., Pollard, D. F., Rettinger, M., Riris, H., Rousogonous, C., Sha, M. K., Shiomi, K., Strong, K., Sussmann, R., Té, Y., Velasco, V. A., Wofsy, S. C., Zhou, M., and Wennberg, P. O.: The Total Carbon Column Observing Network's GGG2020 data version, *Earth Syst. Sci. Data*, 16, 2197–2260, <https://doi.org/10.5194/essd-16-2197-2024>, 2024.
- 435 Masarie, K. A., and Tans, P.P. : Extension and integration of atmospheric carbon dioxide data into a globally consistent measurement record, *J. Geophys. Res.*, 100(D6), 11593–11610, doi:10.1029/95JD00859, 1995.



- Membrive, O., Crevoisier, C., Sweeney, C., Danis, F., Hertzog, A., Engel, A., Bönisch, H., and Picon, L.: AirCore-HR: a high-resolution column sampling to enhance the vertical description of CH<sub>4</sub> and CO<sub>2</sub>, *Atmos. Meas. Tech.*, 10, 2163–2181, <https://doi.org/10.5194/amt-10-2163-2017>, 2017.
- 440 Taylor, T.T. et al : An 11-year record of XCO<sub>2</sub> estimates derived from GOSAT measurements using the NASA ACOS version 9 retrieval algorithm. *Earth Syst. Sci. Data*, 14, 325–360, doi : 10.5194/essd-14-325-2022, 2022.
- Lindqvist, H., O'Dell, C. W., Basu, S., Boesch, H., Chevallier, F., Deutscher, N., Feng, L., Fisher, B., Hase, F., Inoue, M., Kivi, R., Morino, I., Palmer, P. I., Parker, R., Schneider, M., Sussmann, R., and Yoshida, Y.: Does GOSAT capture the true seasonal cycle of carbon dioxide?, *Atmos. Chem. Phys.*, 15, 13023–13040, [https://doi.org/10.5194/acp-15-](https://doi.org/10.5194/acp-15-13023-2015)
- 445 13023-2015, 2015.
- Piao S, Liu Z, Wang Y, et al. On the causes of trends in the seasonal amplitude of atmospheric CO<sub>2</sub>. *Glob Change Biol.* 2018; 24: 608–616. <https://doi.org/10.1111/gcb.13909>
- Reuter, M., Buchwitz, M., Schneising, O., Hase, F., Heymann, J., Guerlet, S., Cogan, A. J., Bovensmann, H., and Burrows, J. P.: A simple empirical model estimating atmospheric CO<sub>2</sub> background concentrations, *Atmos. Meas. Tech.*, 5, 1349–
- 450 1357, <https://doi.org/10.5194/amt-5-1349-2012>, 2012.
- Thoning, K.W., Crotwell A.M., and Mund, J.W.: Atmospheric Carbon Dioxide Dry Air Mole Fractions from continuous measurements at Mauna Loa, Hawaii, Barrow, Alaska, American Samoa and South Pole, 1973-present. Version 2025-04-26, National Oceanic and Atmospheric Administration (NOAA), Global Monitoring Laboratory (GML), Boulder, Colorado, USA <https://doi.org/10.15138/yaf1-bk21>, 2025.
- 455 Thoning, K. W., Tans, P. P., and Komhyr W.D. :), Atmospheric carbon dioxide at Mauna Loa Observatory: 2. Analysis of the NOAA GMCC data, 1974–1985, *J. Geophys. Res.*, 94(D6), 8549–8565, doi:10.1029/JD094iD06p08549, 1989.
- Wunch D., G. C. Toon, J.F. L. Blavier, R. A. Washenfelder, J. Notholt, B. J. Connor, D. W. T. Griffith, V. Sherlock, P. O. Wennberg; The Total Carbon Column Observing Network. *Philos Trans A Math Phys Eng Sci*; 369 (1943): 2087–2112. <https://doi.org/10.1098/rsta.2010.0240>, 2011.